LA-UR-83-3009

CONF-831015--10

LA-UR--83-3009

DE84 001703

TITLE: EFFICIENCY OF A BISMUTH-GERMANATE SCINTILLATOR: COMPARISON OF MONTE CARLO CALCULATIONS WITH MEASUREMENTS

AUTHOR(S): H. H. Hsu, E. J. Dowdy, G. P. Estes, M. C. Lucas, J. M. Mack, and C. E. Moss
Los Alamos National Laboratory

M. E. Hamm
Technical Programming Services

SUBMITTED TO: IEEE 1983 Nuclear Science Symposium
San Francisco, California
October 19-21, 1983

DISCLAIMER

Los Alamos Los Alamos National Laboratory
Los Alamos, New Mexico 87545

FORM NO 836 R4
ST NO 2629 5/81

EFFICIENCY OF A BISMUTH-GERMANATE SCINTILLATOR: COMPARISON OF MONTE CARLO CALCULATIONS WITH MEASUREMENTS*

H. H. Hsu, E. J. Dowdy, G. P. Estes,
M. C. Lucas, J. M. Mack, and C. E. Moss
Los Alamos National Laboratory
Los Alamos, New Mexico 87545

and

M. E. Hamm
Technical Programming Services
Pleasanton, California 94566

Abstract

Monte Carlo calculations of a bismuth-germanate scintillator's efficiency agree closely with experimental measurements. For this comparison, we studied the absolute gamma-ray photopeak efficiency of a scintillator (7.62 cm long by 7.62 cm in diameter) at several gamma-ray energies from 166 to 2615 keV at distances from 0.5 to 152.4 cm. Computer calculations were done in a two-dimensional cylindrical geometry with the Monte Carlo coupled photon-electron code CYLTRAN. For the experiment we measured 11 sources with simple spectra and precisely known strengths. The average deviation between the calculations and the measurements is 3%. Our calculated results also closely agree with recently published calculated results.

Introduction

The inorganic scintillator, bismuth germanate (BGO), has a number of properties that make it an attractive alternative to the widely used sodium iodide for some spectrometry applications that do not require the better resolution of sodium iodide. Our application is one of those cases. We are developing the instruments and measurement methods for obtaining, in situ, spectrally derived dose rates attributable to multiple, spatially extended sources emitting both neutrons and gamma rays in physically complex geometries. As a parallel effort, we are continuing to develop the computational tools to simulate the neutron, photon, and electron transport for these cases. In particular, in part of this program, we are interested in validating the computed results of the transport of photon flux spectra. The specific properties of bismuth germanate that make it attractive for these measurements include a relatively small response to the neutrons in the mixed radiation field (because of the comparatively small neutron cross-sections of the constituent elements) and a large photopeak-to-Compton continuum ratio that results from the higher density of bismuth germanate compared with sodium iodide.

Because the objective of the validation program is to compare calculated and measured photon flux spectra, we have initially chosen the simplest test case to confirm that it is possible to calculate the actual response of one of these scintillators to point gamma-ray sources in free fields. In addition, the response-function matrix for the detector has been developed from interpolations of analytical function fits to the individual measured responses to monoenergetic gamma-rays. Once the response-function matrix is available, the detector pulse-height distributions can be unfolded to provide measured photon flux spectra for comparison with calculated photon flux spectra. We believe this step to be well understood. We are most interested, therefore, in comparisons of the calculated and measured pulse-height distributions.

In the sections that follow, we describe the Monte Carlo code used to calculate the detector response, the measurement methodology, the analytical function fits to the efficiency and resolution parameters, and the comparison of the measured and calculated photon pulse-height distributions.

Calculational Method

To calculate the detector response we employed the code CYLTRAN[1] (coupled TRANsport of electrons and photons in CYLindrical geometry) that combines a condensed-history electron Monte Carlo technique with a conventional single-scattering photon Monte Carlo technique to simulate the transport of all generations of particles (cascade) from several MeV to 1.0 keV for electrons and photons. The model is more accurate at the higher energies, with a less rigorous treatment of the particle cascade at energies where shell structure of the transport media becomes important.

The electron transport includes energy-loss straggling; multiple elastic scattering (angular straggling); and the production of knock-on electrons, continuous bremsstrahlung, characteristic x rays, and annihilation radiation. The photon transport allows photoelectric, Compton, and pair-production interactions, and possible subsequent generation and transport of the corresponding secondary particles. Detailed electron transport is employed down to a preset energy cutoff, at which point the electrons are ranged out along a straight path trajectory. The treatment of photoionization and electron impact ionization, as well as relaxation by fluorescent and Auger processes, are considered only

*This work was supported by the United States Department of Energy.

in the case of the K-shell of the element with the highest atomic number for a given material.

The generation and subsequent transport of the cascade components automatically provide comprehensive energy deposition information. This naturally allows one to tally, for given Monte Carlo cells, the spectrum of absorbed energy from each incident source particle, including the effects of the cascade. The tally answers the following basic question: how much energy is deposited in a region of interest by a given source particle? Thus, a score in this context represents a normalized count within an energy channel of the weight of a particle that loses ΔE as it is transported through the detector volume. With this information, counts (particle weights) can be scored within energy-loss bins (channels) to provide the spectrum of absorbed energy. These data are then folded with an appropriate detector broadening function to yield the pulse-height distribution function. The entire tally procedure closely parallels the operation of a multichannel analyzer.

Experimental Method

Measurement Details

The detector studied contained a 7.62-cm-long by 7.62-cm-diameter bismuth germanate crystal with a resolution of 14.6% (full width at half maximum) at 662 keV. The crystal, supplied by Harshaw Chemical Company, was mounted on a photomultiplier tube in the Harshaw standard integral assembly. The detector was supported on a low-mass tripod at least 1.5 m from the nearest object to minimize scattering effects.

Eleven point sources with simple spectra were used to cover the range from 165.9 to 2614.6 keV: ^{139}Ce, ^{203}Hg, ^{51}Cr, ^{113}Sn, ^{7}Be, ^{85}Sr, ^{137}Cs, ^{54}Mn, ^{65}Zn, ^{88}Y, and ^{208}Tl. The manufacturers who supplied the sources certified their strength. However, for confirmation, we recalibrated the first ten sources with a high-purity germanium detector against a National Bureau of Standards mixed source containing ^{125}Sb, ^{154}Eu, and ^{155}Eu. The intensities of the gamma-ray lines in this mixed source had uncertainties of $\leq$0.7%. We assigned a total uncertainty of 3 to 5% to our source strengths. There was no need to recalibrate the ^{208}Tl source since it was supplied by the National Bureau of Standards with an uncertainty in intensity of the 2614.6-keV line of 2.00%. When used with the BGO detector, each source was suspended by tape to minimize scattering. The calibration distances from the source to the front of the detector were 30.5, 61.0, 91.4, and 152.4 cm, which correspond to distances used in various relevant applications.

The pulse-height distributions were acquired with a LeCroy 3500 data acquisition system. The deadtime was always less than 20% so that pileup and other count-rate effects were insignificant. The measurements took place in the basement of a large concrete building to minimize the interference from experiments in other buildings. Background pulse-height distributions were acquired and used to correct the source pulse-height distributions.

Data Analysis

To determine the experimental photopeak efficiency, it is first necessary to determine the photopeak area. For simple spectra, the sum of the counts in a window containing the photopeak is a good approximation. The window should extend approximately from the minimum between the photopeak and the Compton edge to a point well down on the high-energy tail. This approximation is used in the comparison with the Monte Carlo calculation described in the following section.

The above approximation includes small contributions from the low-energy and high-energy tails. To remove these contributions a Gaussian function with low-energy and high-energy polynomial tails was fitted to the photopeak. The function is given by

$$y(x) = y_0\left\{\exp\left[-(x-x_0)^2/2\sigma\right]\right\}\left[1 + \alpha_1(x-x_0)^4 + \alpha_2(x-x_0)^{12} + \alpha_3(x-x_0)^4 + \alpha_4(x-x_0)^{12}\right],$$

where

y = calculated count in energy channel x,
x_0 = energy channel at the center of the gaussian function,
σ = gaussian width parameter,
α_1, α_2, α_3, α_4 = coefficients of the polynomials,
α_1, α_2 = 0 for $x > x_0$, and
α_3, α_4 = 0 for $x < x_0$.

Figure 1 shows a fit to the 279-keV photopeak from ^{203}Hg. In general, the low-energy tail is significant but the high-energy tail can be ignored. Our experience shows that for complex pulse-height distributions, the tail contributions range from 0.6 to 8.0%, with the larger contribution observed for the lower energy portions of those distributions.

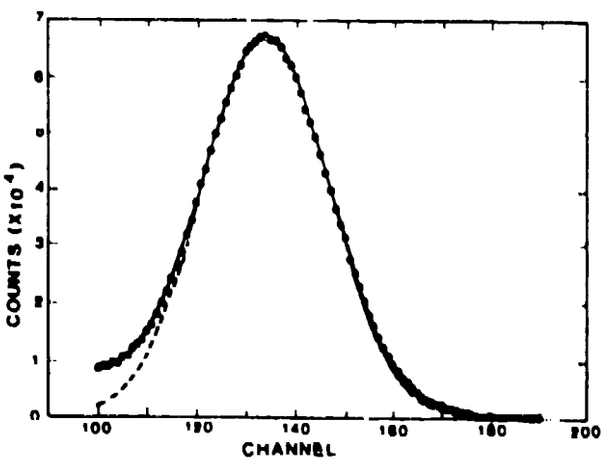

Figure 1
Fit to the photopeak in the pulse-height distribution from ^{203}Hg. The dashed curve is the pure gaussian function; the solid curve is the sum of the gaussian and the polynomials. The measurement data are represented as dots.

For the most accurate determination of the photopeak areas in complex spectra we have used the complete response function as a function of energy. Detailed descriptions of these procedures have been given elsewhere.[2] For the purpose of this report, we have compared only a measured pulse-height distribution with the calculated one for the response to the 662-keV gamma radiation from ^{137}Cs. The measured distribution contains features that result from the presence of a photomultiplier tube and were thus not free-field measurements. Most notable of the features attributable to these surroundings is the prominent backscatter peak observed in the neighborhood of 200 keV in the distribution shown in Fig. 2.

The absolute photopeak efficiency is easily determined from the photopeak area and the source information. The absolute photopeak efficiency is determined by dividing the number of counts in the photopeak by the number of gamma rays with the correct energy emitted by the source. The intrinsic efficiency is given by the absolute efficiency divided by the fractional solid angle subtended by the front face of the detector. The results are listed in the Table.

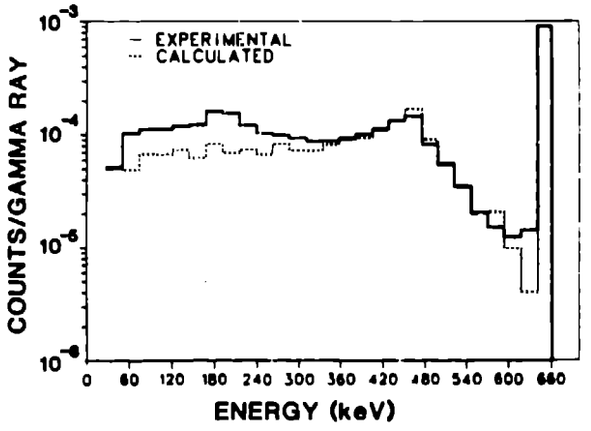

Figure 2
Comparison of the measured and calculated pulse-height distributions for response to the 662-keV gamma rays from ^{137}Cs. The difference at 180 keV results from backscattering not being included in the calculation.

Comparison of Calculations with Measurements

Photons exhibiting specific energy loss in a detector volume are counted in corresponding energy bins (channels) using a multichannel analyzer, which eventually yields a pulse-height distribution. CYLTRAN, using a special tally, simulates the generation of the pulse-height distribution by following the transport details of the photon-electron cascade in multimedia cylindrical geometry. Pulse-height distributions are sensitive to

TABLE

COMPARISON BETWEEN CALCULATED AND EXPERIMENTAL EFFICIENCIES OF A 7.62-cm x 7.62-cm BGO DETECTOR

	Distance Between Source and Detector							
	30.5 cm		61.0 cm		91.4 cm		152.4 cm	
E_γ (MeV)	Calculated ($\times 10^{-3}$)	Experimental ($\times 10^{-3}$)	Calculated ($\times 10^{-4}$)	Experimental ($\times 10^{-4}$)	Calculated ($\times 10^{-4}$)	Experimental ($\times 10^{-4}$)	Calculated ($\times 10^{-4}$)	Experimental ($\times 10^{-4}$)
0.1659	3.32	---	8.56	8.29	3.82	---	1.39	---
0.2792	3.39	3.35	8.83	8.56	3.97	4.11	1.44	1.49
0.3200	---	---	9.01	9.20	---	---	---	---
0.3914	3.28	3.30	8.73	8.70	3.92	---	1.42	---
0.4776	---	---	8.49	8.33	---	---	---	---
0.5140	---	---	8.45	8.64	---	---	---	---
0.6617	2.90	3.04	7.97	8.24	3.64	---	1.34	---
0.8348	2.82	2.82	7.54	7.15	3.45	3.33	1.25	1.20
1.1155	2.46	2.49	6.76	6.81	3.07	---	1.15	---
1.836	---	---	5.51	6.09	---	---	---	---
2.6146	1.68	1.66	4.85	4.41	2.17	2.05	0.797	0.751

the geometry and the materials of the detector. Figure 3 illustrates the CYLTRAN model geometry and materials used in our Monte Carlo simulations; most of this information was verified through the manufacturer. The geometry is cylindrically symmetric about the "dashed line." The 7.6-cm by 7.6-cm BGO crystal has an aluminum case (0.05-cm thick) surrounding the front and lateral sides of the crystal cylinder. Internal to the aluminum at the front of the detector are layers of sponge rubber and polyethylene (0.1-cm thick) that we have assumed to be 100% polyethylene. Finally, there is also a magnesium-oxide reflector (0.2-cm thick) adjacent to the front end and lateral sides of the crystal. Also indicated in Fig. 3 is the point isotropic source at some representative distance from the front face of the detector. Pulse-height distributions were calculated at different source-to-detector distances. The photomultiplier tube is shown for completeness; however, because it contributes less than 20% to the 180° backscatter, it was not explicitly modeled in the Monte Carlo simulations. Similarly, the concrete walls of the room in which the empirical data were acquired were not included in the Monte Carlo simulations.

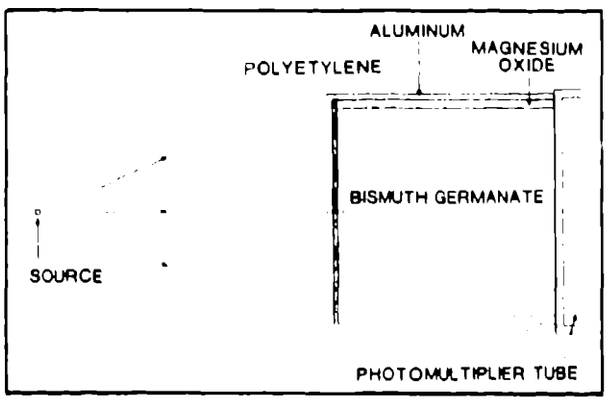

Figure 3
Geometry of the model used for the CYLTRAN code.

The first calculation was the pulse-height distribution for comparison with the measured spectrum. The experimental and calculated results for response to ^{137}Cs gamma rays of 662 keV are shown in Fig. 2. The photopeak and Compton edge agree very well when the following points are considered. In the calculation, the photopeak has a δ-function-like distribution. However, in experimental pulse-height distributions the finite resolution of the detector produces broadened photopeaks. For example, the full width at half maximum of the photopeak for the 662-keV gamma ray from ^{137}Cs is 14.6% in the measured pulse-height distribution. Therefore, in the calculation the photopeak energy bin was extended down to 532 keV for comparison of the detector efficiencies. The experimental area of the photopeak was taken as equal to the sum of the counts between a point well out on the high energy tail and the 532-keV point that is in the valley between the photopeak and the Compton edge of the experimental pulse-height distribution. Because of the manner in which the photopeak area was compared with the experimental value, too many events were allowed in the calculated photopeak, exaggerating the peak-to-valley ratio. These feature differences between the measured and calculated pulse-height distributions are evident in Fig. 2. We are confident that a more accurate accounting of photopeak events would show a much better agreement in this region between the two distributions. The lack of accounting for the backscatter peak in the calculated distribution (discussed above) is also obvious.

Calculations of efficiency were carried out for source-to-detector distances of 30.5, 61.0, 91.4 and 152.4 cm and for gamma-ray energies ranging from 165.9 to 2614.6 keV. The results are summarized in the Table and are also plotted in Fig. 4. The results of calculations and experimental measurements are in

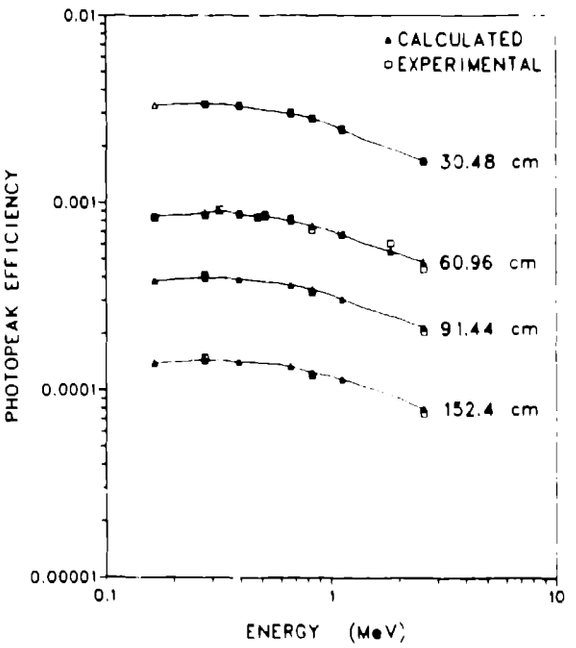

Figure 4
Comparison of the measured and calculated absolute photopeak efficiencies at four source-to-detector distances. The average deviation between the calculations and the measurements is 3%.

excellent agreement. The log-log plots of detector efficiency versus energy are relatively simple and smooth, and can be fitted with the function

$$\ln(\text{eff}) = \sum_{i=1}^{n} C_i \, (\ln E)^{i-1} \quad .$$

Over the energy range of 165.9 to 2614.6 keV, a three-term polynomial suffices in all four cases for agreement within a 3% uncertainty. We list the results of the polynomial fit by increasing distance between the source and the detector (E is the energy of the gamma ray in MeV).

At 30.48 cm,

$$\ln(\text{eff}) = -5.94439 - (0.351874 * \ln E) - [0.121219 * (\ln E)^2].$$

At 60.96 cm,

$$\ln(\text{eff}) = -7.24455 - (0.317178 * \ln E) - [0.116187 * (\ln E)^2].$$

At 91.44 cm,

$$\ln(\text{eff}) = -8.03206 - (0.309594 * \ln E) - [0.12088 * (\ln E)^2].$$

At 152.4 cm,

$$\ln(\text{eff}) = -9.03325 - (0.303561 * \ln E) - [0.122084 * (\ln E)^2].$$

The energy resolution of the BGO detector as a function of gamma-ray energy was determined from experimental pulse-height distributions. Figure 5 is a log-log plot of percent resolution versus gamma-ray energy. Within the energy range of 165.9 to 2614.6 keV it can be described by a simple function

$$\ln(\text{resolution}) = 2.42311 - [0.459364 * \ln(E)],$$

where resolution is expressed as a percentage and energy is in MeV. S. A. Wender[3] reported that for gamma-ray energies above 6 MeV, the resolution is 6% and is limited by the low energy tail due to escape radiation.

D. W. O. Rogers reported Monte Carlo calculations of detector response functions in Ref. 4. His results for the photopeak efficiency for a bare BGO detector with source-to-detector distance of 10 cm are plotted in Fig. 6 along with results from CYLTRAN calculations. The agreement is very good.

Summary

In principle, CYLTRAN also can be used to calculate accurately the ratios of photopeak to first escape peak and photopeak to second escape peak. These numbers can be helpful in resolving experimental photopeaks from escape peaks and in determining the energy resolutions of BGO detectors for gamma rays above 6 MeV.

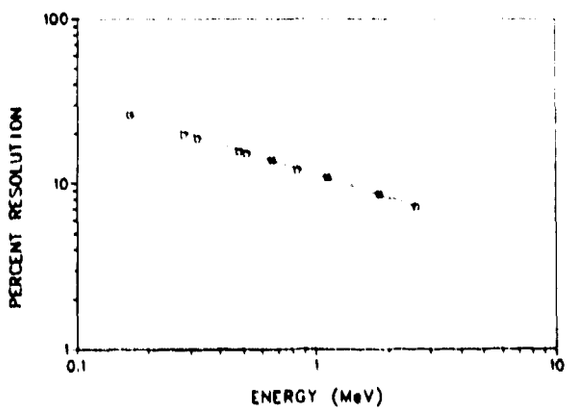

Figure 5
*Plot of the detector resolution as a function of gamma-ray energy. The expression, ln(resolution) = 2.42311 - 0.459364 * ln(energy), is a fit to the experimental data.*

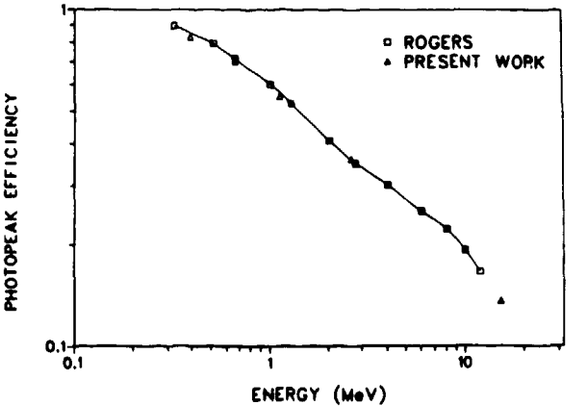

Figure 6
Comparison of the previously reported calculated values of photopeak efficiency versus energy with the present results. The excellent agreement verifies that the results from CYLTRAN and Rogers are consistent.

We have shown that Monte Carlo methods embodied in the computer code CYLTRAN are suitable for the generation of bismuth-germanate detector response functions and photopeak efficiencies. This procedure has been adequately validated by a comparison between a significant body of experimental data and the simulation of those measurement data using the code. The simulation agrees with the comparable measurement to within 3%.

Acknowledgment

We wish to thank Dr. D. W. O. Rogers for providing us with the results of his calculations.

References

[1] J. A. Halbleib, Sr., W. H. Vandevender, "CYLTRAN: A Cylindrical Geometry Multimaterial Electron/Photon Monte Carlo Transport Code," Sandia National Laboratory report SAND-74-0030 (1975), Albuquerque, New Mexico.

[2] C. E. Moss, E. J. Dowdy, A. E. Evans, M. E. Hamm, M. C. Lucas, and E. R. Shunk, "Unfolding Bismuth-Germanate Pulse-Height Distributions to Determine Gamma-Ray Flux and Dose Rates," in "Proceedings of the International Workshop on Bismuth Germanate," Princeton University, Princeton, New Jersey, November 10-13, 1982, to be published in Nuclear Instruments and Methods.

[3] S. A. Wender, "Bismuth Germanate as a High-Energy Gamma-Ray Detector," IEEE Trans. Nucl. Sci. NS-30, 1539 (1983).

[4] D. W. O. Rogers, "More Realistic Monte Carlo Calculations of Photon Detector Response Functions," Nucl. Inst. and Meth. 199, 531 (1982).